Journal Pre-proof

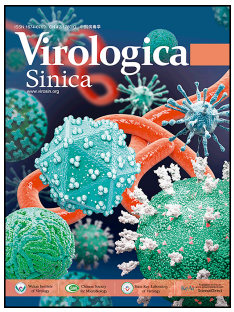

Evolutionary dynamics and comparative pathogenicity of clade 2.3.4.4b H5 subtype avian influenza viruses, China, 2021–2022

Siru Lin, Junhong Chen, Ke Li, Yang Liu, Siyuan Fu, Shumin Xie, Aimin Zha, Aiguo Xin, Xinyu Han, Yuting Shi, Lingyu Xu, Ming Liao, Weixin Jia

PII: S1995-820X(24)00060-9

DOI: https://doi.org/10.1016/j.virs.2024.04.004

Reference: VIRS 273

To appear in: *Virologica Sinica*

Received Date: 26 September 2023

Accepted Date: 18 April 2024

Please cite this article as: Lin, S., Chen, J., Li, K., Liu, Y., Fu, S., Xie, S., Zha, A., Xin, A., Han, X., Shi, Y., Xu, L., Liao, M., Jia, W., Evolutionary dynamics and comparative pathogenicity of clade 2.3.4.4b H5 subtype avian influenza viruses, China, 2021–2022, *Virologica Sinica*, https://doi.org/10.1016/j.virs.2024.04.004.

For article VS6526 (VIRS_273), the author and affiliation list is shown as bellow:

Siru Lin [a, 1], Junhong Chen [a, 1], Ke Li [d, 1], Yang Liu [a, 1], Siyuan Fu [a],Shumin Xie [a], Aimin Zha [a], Aiguo Xin [a], Xinyu Han [a], Yuting Shi [a], Lingyu Xu [a], Ming Liao [a, b, c, *], Weixin Jia [a, b, c, *]

[a] National Avian Influenza Para-Reference Laboratory, Guangdong Engineering Laboratory for Medicament of Zoonosis Prevention and Control, Key Laboratory of Zoonoses Prevention and Control of Guangdong Province, Laboratory for Lingnan Modern Agriculture, College of Veterinary Medicine, South China Agricultural University, Guangzhou, 510642, China

[b] Key Laboratory of Zoonoses, Key Laboratory of Animal Vaccine Development, Ministry of Agriculture, Guangzhou, 510642, China

[c] Key Laboratory of Zoonoses Prevention and Control of Guangdong Province, Guangzhou, 510642, China

[d] Institute of Poultry Management and Diseases, Yunnan Animal Science and Veterinary Institute, Kunming, 650000, China

VS6526

Received: 26 September 2023, Accepted: 18 April 2024

Research article

Evolutionary dynamics and comparative pathogenicity of clade 2.3.4.4b H5 subtype avian influenza viruses, China, 2021–2022

Siru Lin [a, 1], Junhong Chen [a, 1], Ke Li [a, 1], Yang Liu [a, 1], Siyuan Fu [a],Shumin Xie [a], Aimin Zha [a], Aiguo Xin [a], Xinyu Han [a], Yuting Shi [a], Lingyu Xu [a], Ming Liao [a, b, c, *], Weixin Jia [a, b, c, *]

[a] National Avian Influenza Para-Reference Laboratory, Guangdong Engineering Laboratory for Medicament of Zoonosis Prevention and Control, Key Laboratory of Zoonoses Prevention and Control of Guangdong Province, Laboratory for Lingnan Modern Agriculture, College of Veterinary Medicine, South China Agricultural University, Guangzhou, 510642, China

[b] Key Laboratory of Zoonoses, Key Laboratory of Animal Vaccine Development, Ministry of Agriculture, Guangzhou, 510642, China

[c] Key Laboratory of Zoonoses Prevention and Control of Guangdong Province, Guangzhou, 510642, China

[d] Institute of Poultry Management and Diseases, Yunnan Animal Science and Veterinary Institute, Kunming, 650000, China

*Corresponding authors:

Email: jiaweixin@scau.edu.cn (W. Jia); mliao@scau.edu.cn (M. Liao)

ORCID: 0000-0002-6335-9067 (W. Jia); 0000-0001-8731-4528 (M. Liao)

[1] Siru Lin, Junhong Chen, Ke Li, and Yang Liu contributed equally to this article.

Highlights

1. The evolutionary and biological properties of major pandemic H5 AIVs isolated from China in 2021–2022 were analyzed.
2. H5Nx isolates originated from H5N8, with high evolutionary rate in H5N1 and H5N8 and a declining trend in H5N6 in 2015–2022.
3. HI assay suggests that A(H5N1) viruses may be antigenically distinct from the circulating H5N6 and H5N8 strains.
4. Representative viruses of three H5 AIVs isolates exhibit variable tissue tropism and pathogenicity in mice.
5. A(H5N1) viruses have a higher risk of emergence in the future.

Abstract

The recent concurrent emergence of H5N1, H5N6, and H5N8 avian influenza viruses (AIVs) has caused significant avian mortality globally. Since 2020, frequent human-animal interactions have been documented. To gain insight into the novel H5 subtype AIVs (i.e., H5N1, H5N6 and H5N8), we conducted a comparative analysis on phylogenetic evolutionary and biological properties of H5 subtype AIVs strains isolated from China between January 2021 and September 2022. Phylogenetic analysis revealed that the 41 H5Nx strains belonged to clade 2.3.4.4b, with 13 related to H5N1, 19 to H5N6, and 9 to H5N8. The genetic relatedness analysis based on global 2.3.4.4b viruses showed that all the viruses described in this study was likely originated from H5N8, exhibiting a heterogeneous evolutionary history between H5N1 and H5N6 during 2015–2022 worldwide. In this context, we further estimated that H5N1, characterized by higher evolutionary rates in 2021–2022 and more sites under positive selection pressure in 2015–2022. The antigenic profiles of novel H5N1 and H5N6 exhibited notable variations. Further hemagglutination inhibition assay suggest that some A(H5N1) viruses may be antigenically distinct from the circulating H5N6 and H5N8 strains. Mammalian challenge assays demonstrated that the H5N8 virus (21GD001_H5N8) displayed the highest pathogenicity in mice, followed by the H5N1 virus (B1557_H5N1) and then the H5N6 virus (220086_H5N6), suggesting a heterogeneous virulence profile of H5 AIVs in the mammalian hosts. Based on the above results, we consider that A(H5N1) viruses have a higher risk of emergence in the future. Collectively, these findings unveil a new landscape of different evolutionary history and biological characteristics of novel H5 AIVs in clade 2.3.4.4b, contributing to a better understanding for designing more effective strategies for the prevention and control of novel H5 AIVs.

Keywords: Avian influenza virus (AIV)；H5 subtypes AIVs；Evolutionary；Pathogenicity

1 Introduction

The unexpected surge in the prevalence of the H5 subtype avian influenza virus (AIV) from 2021 to 2022 has raised significant global concerns. The epidemics of novel H5N1, H5N6 and H5N8 viruses pose severe threats to the poultry industry, ecosystems and public health worldwide (Chen et al., 2022; Shi and Gao, 2021; Wille and Barr, 2022). H5N8 AIV first emerged in Europe in late 2020, and in May 2021, a human H5N8 virus infection case from Russia was reported (Pyankova et al., 2021). During our routine national surveillance of AIV in May 2021, we found that the hemagglutinin (*HA*) genes of novel H5N6 viruses in the Chinese poultry market were combined with those of H5N8 viruses (Chen et al., 2022). From March to November 2021, the number of novel H5N6 AIV infections and deaths in China dramatically increased, surpassing the total count of the previous seven years. Strikingly, these patients had been directly exposed to these poultries prior to their symptom onset (Bi et al., 2021; Gu et al., 2022; Jiang et al., 2022). Subsequent research revealed a high sequence similarity between the *HA* gene of human-origin H5N6 strains and that of avian-origin H5N6 strains. Importantly, both strains shared the same mutation associated with mammalian susceptibility (Bui et al., 2021; Zhang et al., 2022). Fortunately, the updated version of the vaccine strain played a significant role in controlling the virus at the poultry-human level, preventing widespread human infections. However, in November 2021, there were consecutive outbreaks of the novel H5N1 subtype AIV in North America and Europe, with the virus detected in numerous wild bird carcasses, leading to the culling of large numbers of sick poultry (Günther et al., 2022; Isoda et al., 2022; Kuiken and Cromie, 2022; Lo et al., 2022; Sanogo et al., 2022). Previous research indicates that the current round of novel H5N1 avian influenza viruses carries the *HA* gene of H5N8 virus from clade 2.3.4.4b. Furthermore, mutations at sites 137A and 191I enhance the virus's ability to bind to α-2,6-linked sialic acids, which are human-like receptors (Cui et al., 2022; Ke et al., 2022) . We initially observed the introduction of this AIV subtype into China in domestic geese in November 2021, which subsequently spread to other species at the poultry-human interface.

The H5N1, H5N6 and H5N8 AIVs were previously isolated in distinct clades (Bhat et al., 2015; Bi et al., 2016a, 2016b; Samir et al., 2018; Shi and Gao, 2021; Zhang et al., 2021). However, a remarkable and unusual occurrence is the concurrent presence of these three H5 AIV subtypes within clade 2.3.4.4b. It is worth noting that prior research has confirmed that the novel H5N1 and H5N6 viruses within clade 2.3.4.4b acquired their *HA* genes from H5N8 viruses (Chen et al., 2022; Cui et al., 2022). Nevertheless, the precise evolutionary history and dynamics of these viruses, along with the factors driving their widespread prevalence, remain elusive. Furthermore, there is a need to investigate the co-variation of the biological characteristics of these three AIV subtypes, their potential evolution at the animal-human interface, and the applicability of current prevention and control measures to mitigate the spread of new viruses. Therefore, in this study, we conducted a comprehensive analysis of the evolutionary trajectories of novel H5N1, novel H5N6 and H5N8 viruses, shedding light on the kinetic factors that have led to their extensive spread. Additionally, we evaluated variations in antigenicity and variations in pathogenicity in mice among representative strains of these three AIV subtypes, all of which were collected from China in 2021–2022. Taken together, this present research study delineates the genomic

evolutionary features and biological attributes of the primary prevalent H5 AIVs in clade 2.3.4.4b, offering fresh insights into potential strategies for controlling the virus's dissemination.

2 Materials and methods

2.1 Virus collection and isolation

During our routine surveillance from January 2021 to September 2022 in China, we tested a total of 6102 samples and detected 41 H5-positive samples, including 13 strains of H5N1 AIVs, 19 strains of H5N6 AIVs, and 9 strains of H5N8 AIVs. Ten of the 19 H5N6 subtype AIVs have been reported in our previous studies (https://doi.org/10.3201/eid2808.212241). The hosts primarily consisted of gallinaceous poultry, including chickens, ducks and geese, with a few samples originating from waterfowls and wild birds such as quails and swans. The samples were collected across various regions of China, with a particular focus on the Northeast, North, East, South, Central and Southwest regions, which represent a comprehensive cross-section of the country (Supplementary Table S1). To isolate the viruses, swab samples were mixed with a solution containing 5000 U/mL of penicillin and streptomycin, then inoculated into 9−11-day-old specific pathogen-free (SPF) chicken embryos and placed in a 37 °C incubator for 24–72 hours. Any chicken embryos that perished within the first 24 hours were considered non-specific deaths. The allantoic fluid, harvested from the remaining embryos, was tested for its hemagglutination titer and stored at −80 °C. The *HA* subtype of each virus was determined by haemagglutination inhibition assay using H1−H10 single-factor serum with viral allantoic fluid, while viral NA subtype was determined by PCR assay using N1−N9 detection primers with viral DNA. Viral RNA was extracted using the FastGene kit (Shanghai Feijie Bio-Technology, Shanghai, China), and sample RNA was reverse-transcribed using the Vazyme Reverse Transcription Kit. The PCR products were sent to Shanghai Sangon Biotech for sequencing, which was verified by conducting a BLAST search against the GenBank database.

2.2 Phylogenic analysis

In our previous research, we identified significant clade conversion events in domestic H5 AIVs in China around the year 2016 (Chen et al., 2021). Given that the primary epidemic clade of H5 AIVs has shifted again, we investigated the virus dynamics from 2012−2022 by retrieving global H5 AIV sequences with complete *HA* gene open reading frames from 2012 to 2022 using the GISAID platform (https://platform.gisaid.org/). The sequence datasets were aligned using MAFFT (version 7). To determine the most suitable substitution model, ModelFinder was employed (Kalyaanamoorthy et al., 2017). Subsequently, we utilized IQ-TREE to construct maximum likelihood (ML) phylogenetic trees, which were then visualized using ITOL (version 6, https://itol.embl.de/). To estimate the evolutionary rates, specifically in terms of nucleotide substitutions, of the surface genes of the three AIVs, the BEAST package was employed (version 1.10.4) (Hill and Baele, 2019). To ensure that the datasets exhibited a reliable temporal structure, we assessed the temporal signal of the ML trees using Tempest (version 1.5.3) (Rambaut et al., 2016). We obtained Maximum Clade Credibility (MCC) trees for the HA genes of the three AIV subtypes from 2012 to 2022 using BEAST v1.10 and visualized these trees using FigTree (version 1.4.4). The tree models were all set to Bayesian skyline coalescent, and after the results

were calculated, the viral population dynamics were visualized and analyzed using Tracer v1.7.1.

2.3 Evolutionary rate

In this study, the temporal evolutionary rates of hemagglutinin (*HA*) and neuraminidase (*NA*) genes and the evolutionary rates of epidemic regions for the three subtypes of AIVs from 2015−2022 were estimated using the BEAST package (version 1.10.4).The virus evolutionary rate were visualized and analyzed using Tracer v1.7.1.

2.4 Selection pressure analysis and mutation sites

In contrast, our current study focuses on discerning variations in positive selection pressure experienced by different H5 subtype AIVs, with a specific emphasis on site mutations. For our data analysis, we employed three site models: FEL, FUBAR, and MEME (accessible through Datamonkey; http://www.datamonkey.org/) (Weaver et al., 2018). These models were utilized to assess selection pressure on the *HA* gene of the viruses and to identify codons undergoing positive selection pressure. A *P*-value below 0.10 was considered statistically significant for the FEL model, whereas a *P*-value below 0.90 was considered statistically significant for the FUBAR model. To compare different regions of the viral HA proteins with positive selective pressure, we recorded the sites detected in each model that met the lowest threshold. We analysis Mutation sites by Weblogo 3（http://weblogo.threeplusone.com/）.

2.5 Antigenic analysis

We selected prevalent strains from clade 2.3.4.4b, which were collected between January 2021 and June 2022, for the preparation of antisera. This selection included three strains of H5N1 viruses (designated as B20, B1557 and B149_11), six strains of H5N6 viruses (namely, LD9, B341_4, 220086, 220108, B291_1, D48), and one strain of H5N8 virus (denoted as21GD001). The number of antiserum preparations for each subtype was determined based on the proportion of isolates of the corresponding subtype by taking into account both the timing and location of sample collection. To prepare the antisera, viral allantoic fluid was first inactivated using a 1‰ formaldehyde solution and then emulsified in a 1:1 ratio with Freund's incomplete adjuvant (Zhang et al., 2021). Subsequently, 4-week-old SPF chickens were vaccinated with these preparations, and after four weeks, the sera were collected to assess antibody titers. Antigens and antisera of the vaccine strains were procured from HARVAC (http://www.hvriwk.com/) and SCBM (http://www.gzscbm.com/). The experiments were conducted in accordance with standard protocols, where the antigens to be tested were formulated with four units of virus, and twofold diluted serum samples were added to 96-well plates. The highest serum dilution that resulted in complete inhibition of HA activity was recorded. The hemagglutination inhibition (HI) titers were analyzed using antigenic cartography, a method used to visualize HI cross-reactivity results (Smith et al., 2004).

2.6 Animal experiments

The virus allantoic fluid was introduced into 9–11-day-old specific pathogen-free (SPF) chicken embryos through a tenfold dilution procedure following the limiting dilution method, with each gradient set replicated five times. After 72 hours of incubation, the hemagglutination value of each chicken embryo was determined, and the 50% egg infective dose (EID_{50}) was calculated using the Reed–Muench method (PIZZI, 1950).

Next, we divided 135 BALB/c mice, all aged five weeks, into three groups, representing the three AIV subtypes. Each group was subjected to eight challenge gradients (i.e., 10^1EID_{50}–10^8EID_{50}), with five mice in each gradient. These gradients were determined based on viral EID_{50} to calculate 50% Mouse Lethal Dose (MLD_{50}). Subsequently, we assessed the varying abilities of strains from different subtypes to induce disease in mice. Toxin challenge was administered to each mouse through intranasal inoculation. Mice were considered deceased when their body weight fell below 75% of their initial weight. Additionally, within each subtype, we established a replicate set for the 10^6EID_{50} challenge group (i.e., 10 mice in total), from which three mice each were selected for euthanasia at three and five days post-infection (DPI). Various tissue samples, including the heart, liver, spleen, lung, kidney, brain and nasal concha, were collected from each mouse to determine viral tissue titers.

The various organs were weighed and added to a PBS solution containing 5,000 IU/mL of dual antibody at a ratio of 1 g/1 mL and ground at low temperature. After grinding, each sample was repeatedly freeze-thawed three times and centrifuged at 4,000 r/min for 3 min. The tissue homogenate supernatant was introduced into 9–11-day-old specific pathogen-free (SPF) chicken embryos through a tenfold dilution procedure following the limiting dilution method, with each gradient set replicated three times. After 72 hours of incubation, the hemagglutination value of each chicken embryo was determined, and the 50% egg infective dose (EID_{50}) was calculated using the Reed-Muench method (PIZZI, 1950) as viral tissue titers.

3 Results

3.1 Evolutionary characteristics of H5N1, H5N6, and H5N8 viruses in clade 2.3.4.4b

To examine the genetic relationships of these viruses, we sequenced the genomes of the 41 H5 viruses and constructed maximum-likelihood phylogenetic trees according to the protocol established by the World Health Organization. The H5 subtype avian influenza viruses could be divided into eight clades (clade 2.3.4.4a–h) within clade 2.3.4.4, and all 41 strains in this study belonged to 2.3.4.4b (Fig. 1). According to the ML tree, the currently circulating H5N1, H5N6, and H5N8 AIVs within clade 2.3.4.4b in 2012–2022 are all in clade 2.3.4.4b. (Fig. 1). Regarding spatial and temporal distribution, novel H5N1 AIVs have been observed in circulation in North America and Europe since 2021, with a relatively smaller presence in Asia (Fig. 1). In comparison, H5N8 AIVs were detected in North America and Europe in 2021, while H5N6 AIVs have primarily circulated in Asia since 2021.

3.2 Evolutionary history and phylodynamic analysis of H5N1, H5N6, and H5N8 viruses

According to the MCC tree analysis from 2012 to 2022, we observed that the current novel H5N1 AIVs, H5N6 AIVs and H5N8 AIVs all located in Clade 2.3.4.4b (Fig. 2B). Novel H5N1 begin to appear as cross-branching strains as early as around 2020. The genetic diversity of H5N1 viruses rapidly expanded in 2019 and 2020 (Fig. 2A), followed by an outbreak of H5N1 viruses in 2021(Caliendo et al., 2022; Günther et al., 2022; Shi et al., 2023; Stokstad, 2022). There was a noticeable change in the genetic diversity of H5N6 viruses from 2012 to 2014, followed by a period of stability from 2015 to 2019. Subsequently, the genetic diversity fluctuated over the following four years, coinciding with the emergence of novel H5N6 viruses in China (Fig. 2A). The

H5N8 virus underwent rapid expansion in 2016–2017 following its emergence, after which the population size remained at a consistently high level from 2017 to 2021, which aligns with epidemiological data indicating the endemic status of H5N8 in Europe (Fig. 2A) (Swieton et al., 2020; Verhagen et al., 2021; Zhang et al., 2023) .

Collectively, these findings suggest that the population size of all three AIV subtypes exhibited an upward trend in 2020–2022, following a period of temporal and population-size fluctuations spanning several years.

3.3 Heterogeneous evolutionary rates between H5N1, H5N6, and H5N8 viruses

To understand the genomic mutation dynamics of H5 AIVs, we assessed the evolutionary rates of the *HA* and *NA* genes for each H5 subtype viruses, grouped by different time periods since 2015. We also examined the evolutionary rates of the *HA* gene for each H5 subtype virus, considering geographical differences.

Regarding the H5N1 subtype, the evolutionary rates of the *HA* gene increased from 2015 to 2018, followed by a decrease from 2019 to 2022 (Fig. 3A), with the *NA* gene of H5N1 exhibiting the most pronounced fluctuations compared to the other subtypes (Fig. 3B). In terms of geographical comparisons, the *HA* gene of the H5N1 subtype avian influenza viruses displayed the highest evolutionary rate in North America, potentially due to a close correlation with the recent pandemic of H5N1 subtype AIVs observed in North America in recent years (Fig. 3C).

In contrast, the fluctuation in evolutionary rates for both the *HA* gene and *NA* gene of H5N6 subtype AIVs were under synchronization. Specifically, after a period of accelerated mutation in 2016, both the mutation rates of the *HA* and *NA* genes of H5N6 AIVs decreased in 2017. Subsequently, the evolutionary rates of both genes exhibited an upward trend, reaching a plateau during 2018–2021, followed by a significant decrease in 2022 (Fig. 3A, 3B). Furthermore, it is noteworthy that the evolutionary rate of the viruses was relatively high in Asian regions, including Japan, South Korea, China and Vietnam, while it was relatively low in Europe. This difference may be attributed to variations in the main circulating areas of the virus, suggesting that regional factors may influence the genetic evolution of H5N6 AIVs (Fig. 3C).

Similarly, the fluctuations in the evolutionary rates of the *HA* gene and *NA* gene of H5N8 subtype AIVs were also in synchronicity. Both genes experienced a decrease in their evolutionary rates from 2015 to 2018, followed by an increase in 2019. Subsequently, the mutation rates of both genes recovered in the two subsequent years (Fig. 3A, 3B). Furthermore, it is worth noting that Asia exhibited the highest calculated evolutionary rate compared to the other two continents (Fig. 3C, Supplementary Table S2, S3).

In summary, the evolutionary rates of the two surface genes among the three subtypes of avian influenza viruses remained relatively consistent from 2015 to 2022. Notably, the evolutionary rates of H5N1 and H5N8 viruses were the highest, while the evolutionary rates of H5N6 viruses exhibited a continuing decline over this time frame, possibly influenced by factors such as the main circulating areas and the primary sources of the epidemic. For instance, the evolutionary rate of H5N1 viruses in North America was considerably higher than that observed in other continents. In Asia, the evolutionary rate of H5N6 viruses was significantly higher than in Europe, although it is important to note that there have been no reports of this subtype's existence in North America. Additionally, the H5N8 virus exhibited the highest evolutionary rate in Asian regions.

3.4 Selection pressure analysis

In our analysis, we identified specific sites under positive selection pressure in the *HA* gene of H5N1, H5N6, and H5N8 avian influenza viruses during different time periods in the world. For H5N1, we found 11 sites (four of which are within epitopes) (Peng et al., 2014) under positive selection pressure during 2015–2017, 14 (three of which are within epitopes) during 2017–2019, and 15 (nine of which are within epitopes) during 2019–2022 (Table 1). Similarly, H5N6 had 15 sites (six of which are within epitopes) under positive selection pressure during 2015-2017, 14 (four of which are within epitopes) during 2017–2019, and 10 (three of which are within epitopes) during 2019–2022 (Table 2). In contrast, H5N8 had fewer such sites, with 4 sites (one of which is within epitopes) during 2015–2017, 4 sites (two of which is within epitopes) during 2017–2019, and 3 sites (one of which is within epitopes) during 2019–2022, including some within epitopes (Table 3). Overall, our analysis suggests that the globular domain of the *HA* gene in all three subtypes experienced more selective pressure than the stem region. Additionally, it is worth noting that the epitopes of H5N1 and H5N6 virus *HA* genes were subjected to significantly higher positive selection pressure compared to H5N8 AIVs, implying greater susceptibility to antigenic variation in H5N1 and H5N6 AIVs compared to H5N8 AIVs.

3.5 The mutation characteristic of biased receptor sites and differences in cleavage sites

Between 2021 and 2022, the three subtypes of viruses in the world exhibited notable differences in changes to receptor-associated sites, specifically at H5 numbering. H5N1 viruses displayed alterations at three sites (i.e., 98, 159, and 193), H5N6 viruses at two sites (i.e., 98 and 192), and H5N8 viruses at one site (i.e., 98) (Fig. 4). These sites are linked to the virus's susceptibility and its ability to bind to α-2,6-linked sialic acid receptors. It's worth noting that neither sites 226–228 (Fig. 4), which are associated with susceptibility to avian receptors, nor the cleavage sites of the three H5 AIVs underwent significant changes that would impact the viruses' biological characteristics, as reported in previous studies (Bi et al., 2021; Jiang W et al., 2022) .

3.6 Antigenic characteristics of H5N1, H5N6, and H5N8 viruses in clade 2.3.4.4b

To identify antigenic differences between different subtypes of AIVs within the same clades and compare them to commercial vaccine strains, we conducted HI assays using circulating strains and current commercial vaccine sera. These circulating strains were collected during January 2021 and June 2022 and included H5N1, H5N6, and H5N8 AIVs. Our findings revealed that the current vaccine strains, rHN5801 and Re14, within clade 2.3.4.4b, exhibited strong compatibility with all circulating strains in the same clade (Supplementary Table S4). Conversely, antisera from rGD59 and Re13 vaccine strains within clade 2.3.4.4h lost their protective capacity against all circulating strains in clade 2.3.4.4b (Supplementary Table S4). The HI titers of H5N1 viral antisera (i.e., B20, B1557) against circulating strains of the other two subtypes were notably low (Fig. 5), indicating high antigenic differences between these subtypes. H5N8 viruses exhibited less antigenic divergence from the other two subtypes of AIVs, making them a suitable choice for future vaccine stockpiles within clade 2.3.4.4b. These results underscore the considerable antigenic divergence between H5N1 and H5N6 viruses in clade 2.3.4.4b despite their shared clade classification.

3.7 Pathogenetic assessment of representative viruses of novel H5N1, H5N6 and H5N6 in clade 2.3.4.4b to mammalian

Based on the results of time, location, host distribution, internal genes (Supplementary Table S5) and key

amino acid loci (Supplementary Table S6) of 41 H5 AIVs, we used H5N1 AIV: A/Goose/Henan/B1557/2021 (B1557_H5N1), H5N6 AIV: A/Duck/Chengdu/220086/2022 (220086_H5N6) and H5N8 AIV: A/Chicken/China/21GD001/2021 (21GD001_H5N8) representing H5N1, H5N6, and H5N8 viruses prevalent in China in the period of 2021–2022, to provide a pathogenetic assessment in mice.

Both B1557_H5N1 and 21GD001_H5N8 viruses resulted in 100% mortality, with the exception of the 220086_H5N6 group. Initial mouse fatalities in the novel B1557_H5N1 group occurred at the 10^4 EID_{50} dose, while mice infected with the 220086_H5N6 virus exhibited fatalities starting from at least the 10^6 EID_{50} dose. Comparatively, the 10^2 EID_{50} inoculation with 21GD001_H5N8 virus led to mortality, indicating variable virulence in mammals (Fig. 6A). Based on mortality data from different virus titration gradient groups, we determined the MLD_{50} values for the three H5 subtypes of avian influenza viruses in mice. The MLD_{50} values for the B1557_H5N1 virus, the 220086_H5N6 virus, and the 21GD001_H5N8 virus were 5.17 $Log_{10}EID_{50}$, 6.63 $Log_{10}EID_{50}$, and 2.17 $Log_{10}EID_{50}$, respectively.

High titers of 21GD001_H5N8 virus were detected in the heart, liver, spleen, lung, kidney, brain, and nasal turbinate of mice on 3 DPI after exposure to the 10^6 EID_{50} challenge (viral titers in all tissues except the lung were greater than 3 $\log_{10}$ EID_{50}/100μL), although the viral titer slightly decreased on 5 DPI. The 220086_H5N6 virus was detectable in the heart, liver, spleen, and lung on 3 DPI after inoculation but decreased significantly on 5 DPI (Fig. 6B). The novel B1557_H5N1 virus challenge group showed a similar viral titer compared to the 220086_H5N6 virus challenge group on 3 DPI, whereas the virus could only be detected at a low titer (i.e., 3.41 $\log_{10}EID_{50}$/100μL) in the spleen on 5 DPI.

Collectively, the above results illustrated that H5N8/21 GD001 virus possessed the highest pathogenicity in mice among the three AIVs, followed by the B1557_H5N1 virus then the 220086_H5N6 virus. Furthermore, the H5N8 (21GD001) virus displayed the strongest tissue tropism, followed by the 220086_H5N6 virus then B1557_H5N1 virus.

4 Discussion

The global panzootic outbreak of H5 AIV from 2021 to 2022 has raised significant concerns due to the simultaneous presence of three major subtypes (H5N1, H5N6, and H5N8) within clade 2.3.4.4b, a relatively rare occurrence. These viruses pose a severe threat to both poultry and human public health. As these viruses evolve, changes in their biological characteristics are also notable. The introduction of novel H5N1 and H5N6 AIVs into clade 2.3.4.4b could potentially impact the global H5 AIV ecology, leading to heightened public health concerns. Therefore, there is an urgent need for comprehensive surveillance of H5N1, H5N6, and H5N8 viruses within clade 2.3.4.4b. In our current study, we isolated a total of 41 strains of H5 AIVs, including 13 strains of H5N1, 19 strains of H5N6 and 9 strains of H5N8, from north China (Beijing), east China (Shandong, Anhui, Jiangxi), central China (Henan, Hunan), south China (Guangxi, Guangdong, Hainan), southwest China (Yunnan, Sichuan, Chongqing) and northeast China (Heilongjiang), all belonging to clade 2.3.4.4b. In previous research, H5N1 viruses were classified in clade 2.3.2.1, and H5N6 viruses in clade 2.3.4.4h, whereas only H5N8 was classified in clade 2.3.4.4b, indicating that the current H5N1 and H5N6 viruses have transitioned to the

main epidemic branch. MCC tree results show that the novel H5N1, novel H5N6 and H5N8 viruses share a common origin but have evolved differently. Taken together, the H5N8 virus, as an ancestor of clade 2.3.4.4b, has continuously existed and differentiated from 2015 to 2022. The H5N6 virus began appearing in clade 2.3.4.4b from 2015 to 2020, while the H5N1 virus only emerged in clade 2.3.4.4b in 2021. This suggests that the H5N6 virus started transitioning into clade 2.3.4.4b as early as 2018, compared to the sudden appearance of H5N1 in clade 2.3.4.4b. In addition, as compared to the outbreak of H5N8 in late 2020, the genetic diversity of the H5N1 subtype AIV has already started to increase before 2020. Thus, the outbreak of the novel H5N1 subtype AIV may not be entirely influenced by the H5N8 virus but also by the intense evolution of its own internal groups.

Amid the current global H5N1 outbreak, both surface genes of H5N1 viruses exhibit relatively high evolutionary rates, with the highest rate observed in the *HA* gene within North America, suggesting that H5N1 viruses may possess a stronger evolutionary potential. However, it is also important to note that while the H5N8 virus currently exhibits a high rate of evolution, it may not hold promising epidemic prospects because the H5N8 virus comprises over 95% of sequences from 2021 in the 2021–2022 dataset, indicating that the evolutionary rate for that period may be more representative of 2021 rather than 2021–2022. Furthermore, the global isolation of H5N8 viruses significantly declined in 2022. Therefore, it is plausible to speculate that the evolutionary rate of H5N8 viruses may have also declined, which could be confirmed in the upcoming 2022–2023 datasets. The primary driver behind changes in nucleotide substitution rates is the accumulation of site mutations, and single-locus mutations may benefit from the selection pressure they experience. Between 2019 and 2022, the number of sites under positive selection pressure in the *HA* gene epitopes of H5N1 viruses is notably higher than that observed in H5N1 viruses before 2019, followed by H5N6 viruses, and finally H5N8 viruses. This suggests that H5N1 viruses may have a greater potential for antigenic drift compared to the other two subtypes, signifying that they possess more sites that can undergo substitutions to evade vaccine immunity. Overall, A(H5N1) viruses have a higher risk of emergence in the future compared to other H5 subtypes of AIVs.

The three subtypes of AIVs have displayed varying degrees of adaptive changes in the α-2,6-linked sialic acid receptor-associated sites (Bi et al., 2021; Huang et al., 2021; Xiao et al., 2021; Zhang et al., 2023), implying that these viruses may have an increased potential for infecting mammals, which underscores the importance of strengthening preventive measures to minimize the risk of virus spillover from avian to human populations. Regarding antigenicity, H5N1 virus sera exhibit lower reactivity with the other two subtypes, and H5N1 viruses demonstrate antigenic divergence from certain H5N6 viruses. Therefore, it may be necessary to categorize "targeted" vaccine candidates by subtypes for different subtypes of AIV in clade 2.3.4.4b in the future. Animal experiments have revealed varying degrees of pathogenicity in mice for representative virus of the three H5 AIVs currently circulating in China, with 21GD001_H5N8 virus being the most pathogenic, followed by B1557_H5N1 virus, while 220086_H5N6 virus exhibits the lowest pathogenicity. Strong pathogenicity is not conducive to virus spread when human interventions are employed to control its transmission. For instance, if a virus poses a threat to humans similar to the H7N9 virus, it may expedite the rapid clearance of such viruses from the public health system (Shi et al., 2018, 2017). Therefore, the less pathogenic H5N1/B1557 virus and

220086_H5N6 virus in mice (mammals) might exhibit more subtle transmission characteristics than 21GD001_H5N8 virus, making them more likely to cause widespread epidemics in mammals.

5 Conclusions

In this study, we found that the current novel H5N1 and H5N6 viruses have transitioned to the main pandemic clade (Clade 2.3.4.4b). Three H5 subtypes share a common origin but have evolved differently. Novel H5N1 viruses may have greater antigenic drift potential and more sites where substitution can occur to evade vaccine immunity. Representative viruses of the three H5 subtypes AIVs circulating in China from 2021 to 2022 are pathogenic to mice to varying degrees, with the 21GD001_H5N8 virus being the most pathogenic, followed by the B1557_H5N1 virus, and the 220086_H5N6 virus the least pathogenic. Based on the results above, we consider that A(H5N1) viruses have a higher risk of emergence in the future. However, it is important to acknowledge that this research has its limitations. While we conducted bioinformatics analysis on global sequences available in the GISAID database, the strains used in our antigenicity analysis and animal experiments were sourced exclusively from China and may not fully represent the diversity of global H5N1, H5N6, and H5N8 viruses. Given the current unprecedented fluctuations in H5 subtype AIVs, it is imperative to intensify surveillance efforts aimed at detecting antigenic mutations promptly, which could enable the timely development of vaccine strains to mitigate the potential consequences of antigenic variation and curb further viral dissemination.

Data availability

Background information and sequences of the 41 H5 subtype avian influenza viruses in this study are available in the GISAID database: https://gisaid.org/.

Ethics statement

All experiments with all available influenza A(H5) viruses were conducted in an animal biosafety level 3 laboratory and animal facility under South China Agricultural University (SCAU) (CNAS BL0011) protocols. All animals involved in experiments were reviewed and approved by the Institution Animal Care and Use Committee at SCAU and treated in accordance with the guidelines (2017A002).

Author contributions

Siru Lin: conceptualization, methodology, software, data curation, writing-original draft, writing-review and editing. Junhong Chen: conceptualization, methodology, software, data curation, writing-original draft, writing-review and editing. Shumin Xie: visualization, investigation. Ke Li: software, validation. Yang Liu: software, data curation. Yuxin Zhang: software, data curation. Aimin Zha: software, data curation. Aiguo Xin: software. Lingyu Xu: software. Xinyu Han: writing-original draft. Yuting Shi: writing-original draft. Yaozong Lin: writing-original draft. Ming Liao: conceptualization, funding acquisition, project administration, supervision, resources and validation. Weixin Jia: conceptualization, funding acquisition, project administration,

supervision, resources and validation.

Conflicts of Interest

All authors declare that there are no competing interests.

Acknowledgments

This research was supported by the Science and Technology Program of Guangdong Province (2022B1111010004, 2021B1212030015), China Agriculture Research System of MOF and MARA (CARS-41), China National Animal Disease Surveillance and Epidemiological Survey Program (2021–2025) (No. 202111).

Appendix A. Supplementary data

Supplementary data to this article can be found online at https://do i.org/10.1016/j.virs.####.

References:

Bhat, S., Bhatia, S., Pillai, A.S., Sood, R., Singh, V.K., Shrivas, O.P., Mishra, S.K., Mawale, N., 2015. Genetic and antigenic characterization of H5N1 viruses of clade 2.3.2.1 isolated in India. Microb Pathog 88, 87–93.

Bi, F., Jiang, L., Huang, L., Wei, J., Pan, X., Ju, Y., Mo, J., Chen, M., Kang, N., Tan, Y., Li, Y., Wang, J., 2021. Genetic Characterization of Two Human Cases Infected with the Avian Influenza A (H5N6) Viruses-Guangxi Zhuang Autonomous Region, China, 2021. China CDC Wkly 3, 923–928.

Bi, Y., Chen, J., Zhang, Z., Li, M., Cai, T., Sharshov, K., Susloparov, I., Shestopalov, A., Wong, G., He, Y., Xing, Z., Sun, J., Liu, D., Liu, Y., Liu, L., Liu, W., Lei, F., Shi, W., Gao, G.F., 2016a. Highly pathogenic avian influenza H5N1 Clade 2.3.2.1c virus in migratory birds, 2014–2015. Virol Sin 31, 300–305.

Bi, Y., Chen, Q., Wang, Q., Chen, J., Jin, T., Wong, G., Quan, C., Liu, J., Wu, J., Yin, R., Zhao, L., Li, M., Ding, Z., Zou, R., Xu, W., Li, H., Wang, H., Tian, K., Fu, G., Huang, Y., Shestopalov, A., Li, S., Xu, B., Yu, H., Luo, T., Lu, L., Xu, X., Luo, Y., Liu, Y., Shi, W., Liu, D., Gao, G.F., 2016b. Genesis, Evolution and Prevalence of H5N6 Avian Influenza Viruses in China. Cell Host Microbe 20, 810–821.

Bui, C.H.T., Kuok, D.I.T., Yeung, H.W., Ng, K.C., Chu, D.K.W., Webby, R.J., Nicholls, J.M., Peiris, J.S.M., Hui, K.P.Y., Chan, M.C.W., 2021. Risk assessment for highly pathogenic avian influenza a(H5N6/H5N8) Clade 2.3.4.4 Viruses. Emerg Infect Dis 27, 2619–2627.

Caliendo, V., Lewis, N.S., Pohlmann, A., Baillie, S.R., Banyard, A.C., Beer, M., Brown, I.H., Fouchier, R.A.M., Hansen, R.D.E., Lameris, T.K., Lang, A.S., Laurendeau, S., Lung, O., Robertson, G., van der Jeugd, H., Alkie, T.N., Thorup, K., van Toor, M.L., Waldenström, J., Yason, C., Kuiken, T., Berhane, Y., 2022. Transatlantic spread of highly pathogenic avian influenza H5N1 by wild birds from Europe to North America in 2021. Sci Rep 12, 11729.

Chen, J., Li, X., Xu, L., Xie, S., Jia, W., 2021. Health threats from increased antigenicity changes in H5N6-dominant subtypes, 2020 China. J Infect 83, e9-e11.

Chen, J., Xu, L., Liu, T., Xie, S., Li, K., Li, X., Zhang, M., Wu, Y., Wang, X., Wang, J., Shi, K., Niu, B., Liao, M., Jia, W., 2022. Novel Reassortant Avian Influenza A(H5N6) Virus, China, 2021. Emerg Infect Dis 28, 1701–1707.

Cui, P., Shi, J., Wang, C., Zhang, Y., Xing, X., Kong, H., Yan, C., Zeng, X., Liu, L., Tian, G., Li, C., Deng, G., Chen, H., 2022. Global dissemination of H5N1 influenza viruses bearing the clade 2.3.4.4b HA gene and biologic analysis of the ones detected in China. Emerg Microbes Infect 11, 1693–1704.

Gu, W., Shi, J., Cui, P., Yan, C., Zhang, Yaping, Wang, C., Zhang, Yuancheng, Xing, X., Zeng, X., Liu, L., Tian,

G., Suzuki, Y., Li, C., Deng, G., Chen, H., 2022. Novel H5N6 reassortants bearing the clade 2.3.4.4b HA gene of H5N8 virus have been detected in poultry and caused multiple human infections in China. Emerg Microbes Infect 11, 1174–1185.

Günther, A., Krone, O., Svansson, V., Pohlmann, A., King, J., Hallgrimsson, G.T., Skarphéðinsson, K.H., Sigurðardóttir, H., Jónsson, S.R., Beer, M., Brugger, B., Harder, T., 2022. Iceland as Stepping Stone for Spread of Highly Pathogenic Avian Influenza Virus between Europe and North America. Emerg Infect Dis 28, 2383–2388.

Hill, V., Baele, G., 2019. Bayesian Estimation of Past Population Dynamics in BEAST 1.10 Using the Skygrid Coalescent Model. Mol Biol Evol 36, 2620–2628.

Huang, J., Wu, S., Wu, W., Liang, Y., Zhuang, H., Ye, Z., Qu, X., Liao, M., Jiao, P., 2021. The Biological Characteristics of Novel H5N6 Highly Pathogenic Avian Influenza Virus and Its Pathogenesis in Ducks. Front Microbiol 12, 628545.

Isoda, N., Onuma, M., Hiono, T., Sobolev, I., Lim, H.Y., Nabeshima, K., Honjyo, H., Yokoyama, M., Shestopalov, A., Sakoda, Y., 2022. Detection of New H5N1 High Pathogenicity Avian Influenza Viruses in Winter 2021–2022 in the Far East, Which Are Genetically Close to Those in Europe. Viruses 14, 2168.

Jiang W, Dong C, Liu S, Peng C, Yin X, Liang S, Zhang L, Li J, Yu X, Li Y, Wang J, Hou G, Zeng Z, Liu H, 2022. Emerging Novel Reassortant Influenza A(H5N6) Viruses in Poultry and Humans, China, 2021. Emerg Infect Dis 28, 1064–1066.

Kalyaanamoorthy, S., Minh, B.Q., Wong, T.K.F., Von Haeseler, A., Jermiin, L.S., 2017. ModelFinder: Fast model selection for accurate phylogenetic estimates. Nat Methods 14, 587–589.

Ke, X., Yao, Z., Tang, Y., Yang, M., Li, Y., Yang, G., Chen, J., Chen, G., Feng, W., Zheng, H., Chen, Q., 2022. Highly Pathogenic Avian Influenza A (H5N1) Virus in Swans, Central China, 2021. Microbiol Spectr 10.

Kuiken, T., Cromie, R., 2022. Protect wildlife from livestock diseases. Science 738, 5.

Lo，Fatou T., Zecchin, B., Diallo, A.A., Racky, O., Tassoni, L., Diop Aida, Diouf, Moussa, Diouf, Mayékor, Samb, Y.N., Ambra, P., Federica, G., Ellero, F., Diop, M., Lo, M.M., Diouf, M.N., Fall, M., Ndiaye, A.A., Ndumu, D.B., Gaye, A.M., Badiane, M., Lo, M., Youm, B.N., Ndao, I., Niaga, M., Terregino, C., Diop, B., Ndiaye, Y., Angot, A., Seck, I., Niang, M., Soumare, B., Fusaro, A., Monne, I., 2022. Intercontinental Spread of Eurasian Highly Pathogenic Avian Influenza A(H5N1) to Senegal. Emerg Infect Dis 28, 234–237.

Peng, Y., Zou, Y., Li, H., Li, K., Jiang, T., 2014. Inferring the antigenic epitopes for highly pathogenic avian influenza H5N1 viruses. Vaccine 32, 671–676.

PIZZI, M., 1950. Sampling variation of the fifty percent end-point, determined by the Reed-Muench (Behrens) method. Hum Biol 22, 150–190.

Pyankova, O.G., Susloparov, I.M., Moiseeva, A.A., Kolosova, N.P., Onkhonova, G.S., Danilenko, A. V., Vakalova, E. V., Shendo, G.L., Nekeshina, N.N., Noskova, L.N., Demina, J. V., Frolova, N. V., Gavrilova, E. V., Maksyutov, R.A., Ryzhikov, A.B., 2021. Isolation of clade 2.3.4.4b A(H5N8), a highly pathogenic avian influenza virus, from a worker during an outbreak on a poultry farm, Russia, December 2020. Euro Surveill 26, 2100439.

Rambaut, A., Lam, T.T., Carvalho, L.M., Pybus, O.G., 2016. Exploring the temporal structure of heterochronous sequences using TempEst (formerly Path-O-Gen). Virus Evol 2, vew007.

Samir, M., Hamed, M., Abdallah, F., Kinh Nguyen, V., Hernandez-Vargas, E.A., Seehusen, F., Baumgärtner, W., Hussein, A., Ali, A.A.H., Pessler, F., 2018. An Egyptian HPAI H5N1 isolate from clade 2.2.1.2 is highly pathogenic in an experimentally infected domestic duck breed (Sudani duck). Transbound Emerg Dis 65, 859–873.

Sanogo, I.N., Djegui, F., Akpo, Y., Gnanvi, C., Dupré, G., Rubrum, A., Jeevan, T., McKenzie, P., Webby, R.J., Ducatez, M.F., 2022. Highly Pathogenic Avian Influenza A(H5N1) Clade 2.3.4.4b Virus in Poultry, Benin, 2021. Emerg Infect Dis 28, 2534–2537.

Shi, J., Deng, G., Kong, H., Gu, C., Ma, S., Yin, X., Zeng, X., Cui, P., Chen, Y., Yang, H., Wan, X., Wang, X., Liu, L., Chen, P., Jiang, Y., Liu, J., Guan, Y., Suzuki, Y., Li, M., Qu, Z., Guan, L., Zang, J., Gu, W., Han, S., Song, Y., Hu, Y., Wang, Z., Gu, L., Yang, W., Liang, L., Bao, H., Tian, G., Li, Y., Qiao, C., Jiang, L., Li, C., Bu, Z., Chen, H., 2017. H7N9 virulent mutants detected in chickens in China pose an increased threat to humans. Cell Res 27, 1409–1421.

Shi, J., Deng, G., Ma, S., Zeng, X., Yin, X., Li, M., Zhang, B., Cui, P., Chen, Y., Yang, H., Wan, X., Liu, L., Chen, P., Jiang, Y., Guan, Y., Liu, J., Gu, W., Han, S., Song, Y., Liang, L., Qu, Z., Hou, Y., Wang, X., Bao, H., Tian, G., Li, Y., Jiang, L., Li, C., Chen, H., 2018. Rapid Evolution of H7N9 Highly Pathogenic Viruses that Emerged in China in 2017. Cell Host Microbe 24, 558-568.e7.

Shi, J., Zeng, X., Cui, P., Yan, C., Chen, H., 2023. Alarming situation of emerging H5 and H7 avian influenza and effective control strategies. Emerg Microbes Infect 12, 2155072.

Shi, W., Gao, G.F., 2021. Emerging H5N8 avian influenza viruses: The global spread of H5N8 avian influenza viruses is a public health concern. Science 372, 784-786.

Smith, D.J., Lapedes, A.S., de Jong, J.C., Bestobroer, T.M., Rimmelzwaan, G.F., Osterhaus, A.D.M.E., Fouchier, R.A.M., 2004. Mapping the antigenic and genetic evolution of influenza virus. Science 305, 371–374.

Stokstad, E., 2022. Deadly bird flu establishes a foothold in North America. Science 377, 912.

Swieton, E., Fusaro, A., Fusaro, A., Shittu, I., Niemczuk, K., Zecchin, B., Joannis, T., Bonfante, F., Mietanka, K., Terregino, C., 2020. Sub-Saharan Africa and Eurasia Ancestry of Reassortant Highly Pathogenic Avian Influenza A(H5N8) Virus, Europe, December 2019. Emerg Infect Dis 26, 1557–1561.

Verhagen, J.H., Fouchier, R.A.M., Lewis, N., 2021. Highly Pathogenic Avian Influenza Viruses at the Wild-Domestic Bird Interface in Europe: Future Directions for Research and Surveillance. Viruses 13, 212.

Weaver, S., Shank, S.D., Spielman, S.J., Li, M., Muse, S. V., Kosakovsky Pond, S.L., 2018. Datamonkey 2.0: A modern web application for characterizing selective and other evolutionary processes. Mol Biol Evol 35, 773–777.

Wiley, D.C., Wilson, I.A., Skehel, J.J., 1981. Structural identifcation of the antibody-binding sites of Hong Kong influenza haemagglutinin and their involvement in antigenic variation, 25. Lazarowitz, S. G. & Choppin, P. W. Virology 289, 2737–2740.

Wille, M., Barr, I.G., 2022. Resurgence of avian influenza virus. Science 376, 459–460.

Xiao, C., Xu, J., Lan, Y., Huang, Z., Zhou, L., Guo, Y., Li, X., Yang, L., Gao, G. F., Wang, D., Liu, W. J., Zhou, X., Yang, H., 2021. Five Independent Cases of Human Infection with Avian Influenza H5N6-Sichuan Province, China, 2021. China CDC Wkly 3, 751–756.

Yamashita, A., Kawashita, N., Kubota-Koketsu, R., Inoue, Y., Watanabe, Y., Ibrahim, M.S., Ideno, S., Yunoki, M., Okuno, Y., Takagi, T., Yasunaga, T., Ikuta, K., 2010. Highly conserved sequences for human neutralization epitope on hemagglutinin of influenza A viruses H3N2, H1N1 and H5N1: Implication for human monoclonal antibody recognition. Biochem Biophys Res Commun 393, 614–618.

Zhang, C., Wang, Z.Y., Cui, H., Chen, L.G., Zhang, C.M., Chen, Z.L., Dong, S.S., Zhao, K., Fu, Y.Y., Liu, J.X., Guo, Z.D., 2023. Emergence of H5N8 avian influenza virus in domestic geese in a wild bird habitat, Yishui Lake, north central China. Virol Sin 38, 157–161.

Zhang, G., Li, B., Raghwani, J., Vrancken, B., Jia, R., Hill, S.C., Fournié, G., Cheng, Y., Yang, Q., Wang, Y., Wang, Z., Dong, L., Pybus, O.G., Tian, H., 2023. Bidirectional Movement of Emerging H5N8 Avian Influenza Viruses between Europe and Asia via Migratory Birds since Early 2020. Mol Biol Evol 40,

msad019.

Zhang, J., Li, X., Wang, X., Ye, H., Li, B., Chen, Y., Chen, J., Zhang, T., Qiu, Z., Li, H., Jia, W., Liao, M., Qi, W., 2021. Genomic evolution, transmission dynamics, and pathogenicity of avian influenza A (H5N8) viruses emerging in China, 2020. Virus Evol 7, veab046.

Zhang J, Ye H, Liu Y, Liao M, QI W, 2022. Resurgence of H5N6 avian influenza virus in 2021 poses new threat to public health. Lancet Microbe 3, e558.

532 **Table 1 Positive selection pressure experienced by the *HA* gene of H5N1 subtype avian influenza viruses.**

H5N1	Epitopes					Other
	A	B	C	D	E	
2015–2017	-	152/156	282	170	-	10/47/82/204/205/461/503
2017–2019	-	84/152	-	170	-	4/10/11/30/82/84/104/205/220/286/304/490
2019–2022	-	156/157	45	170/178/205/208/214/234	-	3/18/111/298/339/506

533 Note: Positive selection pressure on the *HA* gene was assessed by dividing the data into three time segments.
534 The epitope regions (A–D) were based on Yamashita's research and Dzimianski's research (Wiley et al., 1981;
535 Yamashita et al., 2010), while other regions were grouped under the "other" category.

536

537 **Table 2 Positive selection pressure experienced by the *HA* gene of H5N6 subtype avian influenza viruses.**

H5N6	Epitopes					Other
	A	B	C	D	E	
2015–2017	131/143/145	152/154/165	-	-	-	3/10/147/150/237/246/323/386/546
2017–2019	137/145	161	-	202	-	97/99/147/150/198/237/299/349/469/519
2019–2022	136	184	-	325	-	9/32/39/325/340/379/491

538 Note: Positive selection pressure on the HA gene was assessed by dividing the data into three time segments.
539 The epitope regions (A–D) were based on Yamashita's research and Dzimianski's research (Wiley et al., 1981;
540 Yamashita et al., 2010) , while other regions were grouped under the "other" category.

541

542 **Table 3 Positive selection pressure experienced by the *HA* gene of H5N8 subtype avian influenza viruses.**

H5N8	Epitopes					Other
	A	B	C	D	E	
2015–2017	139	-	-	-	-	30/99/492
2017–2019	-	-	-	-	88/113	191/565
2019–2022	-	-	-	-	88	538/548

543 Note: Positive selection pressure on the HA gene was assessed by dividing the data into three time segments.
544 The epitope regions (A–D) were based on Yamashita's research and Dzimianski's research (Wiley et al., 1981;
545 Yamashita et al., 2010), while other regions were grouped under the "other" category.

546 **Figure Legends**

547
548

549 **Figure 1.** Global phylogeny of Clade 2.3.4.4b H5 subtype avian influenza viruses, 2020–2022. Analysis of the
550 *HA* genes of H5 subtype influenza viruses within clade 2.3.4.4b during 2012–2022. In the evolutionary tree, red
551 dots indicate H5 isolates from this study; various clade colors denote different subclades; and colored
552 rectangular bars on the right side of the tree indicate continents, subtypes, years, and hosts corresponding to
553 strains at respective locations on the tree. The scale bar represents the number of nucleotide substitutions per
554 site (sub / site).

555
556

557 **Figure 2.** Evolutionary history and phylogenetic dynamics of H5N1, H5N6 and H5N8 viruses, 2015–2022. **A**
558 illustrates the population dynamics of three H5 subtypes of avian influenza viruses. The horizontal axis
559 represents the year, while the vertical axis represents the nucleotide replacement rate. **B** displays the MCC trees
560 of three H5 subtypes of avian influenza viruses spanning from 2012 to 2022. The horizontal axis at the bottom
561 signifies time. Different colors denote distinct evolutionary branches, with black representing H5N6, blue
562 representing H5N1, and pink representing H5N8.

563
564

565 **Figure 3.** Evolutionary rate of the surface genes of three subtypes of avian influenza viruses. **A** illustrates the
566 evolutionary rate of the *HA* gene in different time periods. **B** displays the evolutionary rate of the *NA* gene during
567 various time periods. **C** showcases the evolution rate of different H5 subtypes of avian influenza viruses across
568 different epidemic areas. These regions are categorized based on the primary epidemic areas of various subtypes
569 (refer to Supplementary Table S2 and Table S3 for further details).

570
571

572 **Figure 4.** Characteristics of changes in the receptor preference of associated sites in the *HA* gene of three
573 subtypes of avian influenza viruses. **A** The left panels represent the initial states of the three H5 subtype avian
574 influenza viruses at receptor-associated sites in 2015–2019. **B** The right panels illustrate the states of the three
575 H5 subtype avian influenza viruses at receptor-associated sites in 2021–2022. In both sets of panels, the upper
576 sites, arranged laterally for each subtype, represent mammalian receptor binding-associated sites. Conversely,
577 all the lower-layer sites signify cleavage sites and avian receptor binding-associated sites. The red arrows
578 highlight sites that have undergone significant changes. The abscissa denotes the site position, while the ordinate
579 indicates the frequency at which the same position is occupied by different numbers of amino acids across the
580 dataset.

581
582

583 **Figure 5.** Antigenic characteristics of H5 subtype avian influenza viruses in clade 2.3.4.4b. Antigenic

584 cartography of H5 subtype avian influenza viruses isolated in China. In the diagram, circles symbolize antigens,
585 and squares denote antisera. The separation between circles reflects the antigenic distance, signifying antigenic
586 differences. The distance from the circle to the square indicates the serum's capacity to neutralize the antigen,
587 with a greater distance indicating a weaker serum binding affinity to the antigen. In addition, the coffee-colored
588 squares represent antigens from commercial vaccine strains, the blue circles represent antibodies generated by
589 commercial vaccine strains, the green signifies antigens from epidemic strains, and the transparent squares
590 represent antibodies generated by epidemic strains.

591
592

593 **Figure 6.** Characteristics of the pathogenicity of representative virus of the three H5 subtypes AIVs for
594 mammals. **A** features the survival curve of mice in the 10^1-10^8 EID_{50} challenge group. The x-axis represents
595 days post-challenge, while the y-axis represents survival. In this panel, the blue line depicts the survival curve
596 of mice challenged the representative virus of H5N1 virus (B1557), the yellow line represents the survival curve
597 of mice challenged with the representative virus of H5N6 virus (220086), and the pink line represents the
598 survival curve of mice challenged with the representative virus of H5N8 virus (21GD001). **B** Mice were
599 challenged with the representative virus (10^6 EID_{50}) from three H5 subtypes [A/Goose/Henan/B1557/2021
600 (B1557_H5N1), A/Duck/Chengdu/220086/2022 (220086_H5N6), A/Chicken/China/21GD001/2021
601 (21GD001_H5N8)]. The virus titers in organ tissues collected from mice on day 3 and day 5 were titrated by
602 determining the 50% egg infective dose (EID_{50}). The EID_{50} was calculated using the Reed-Muench method.

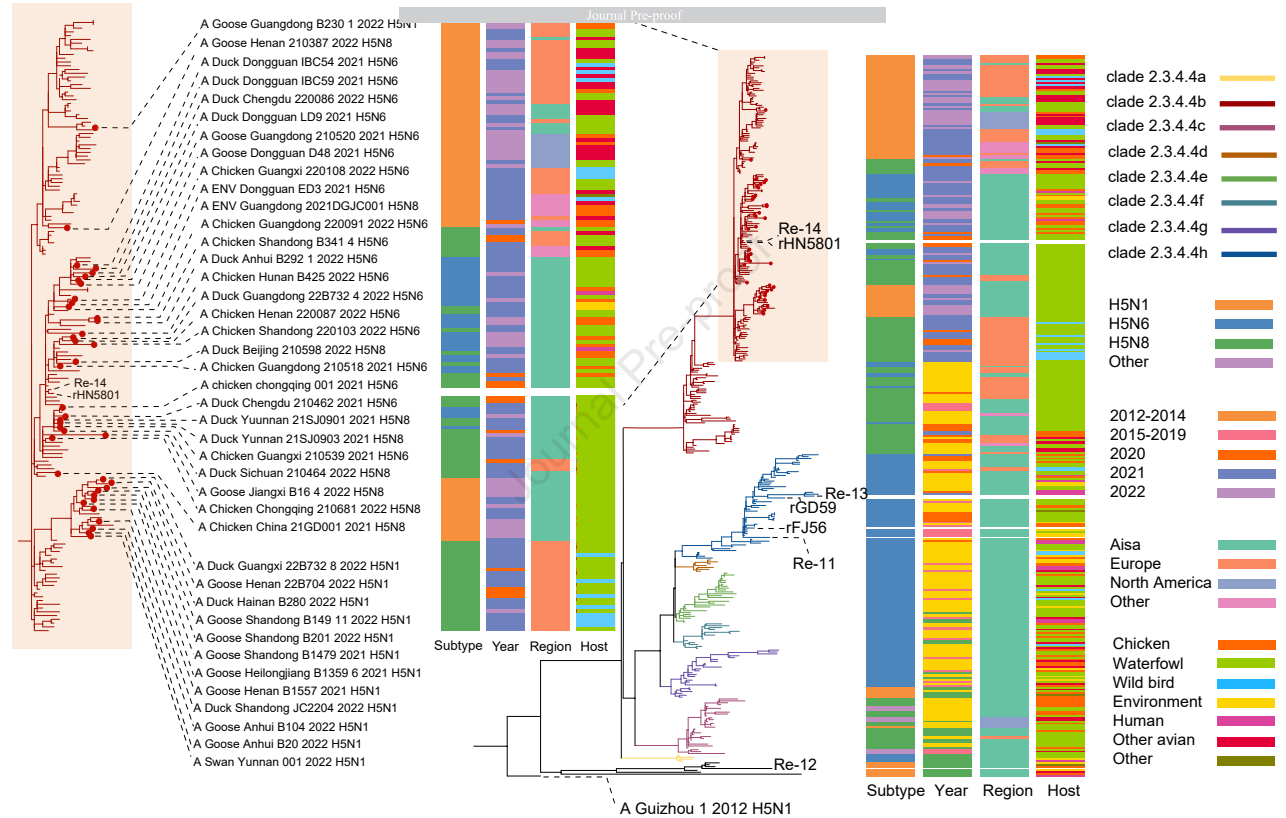

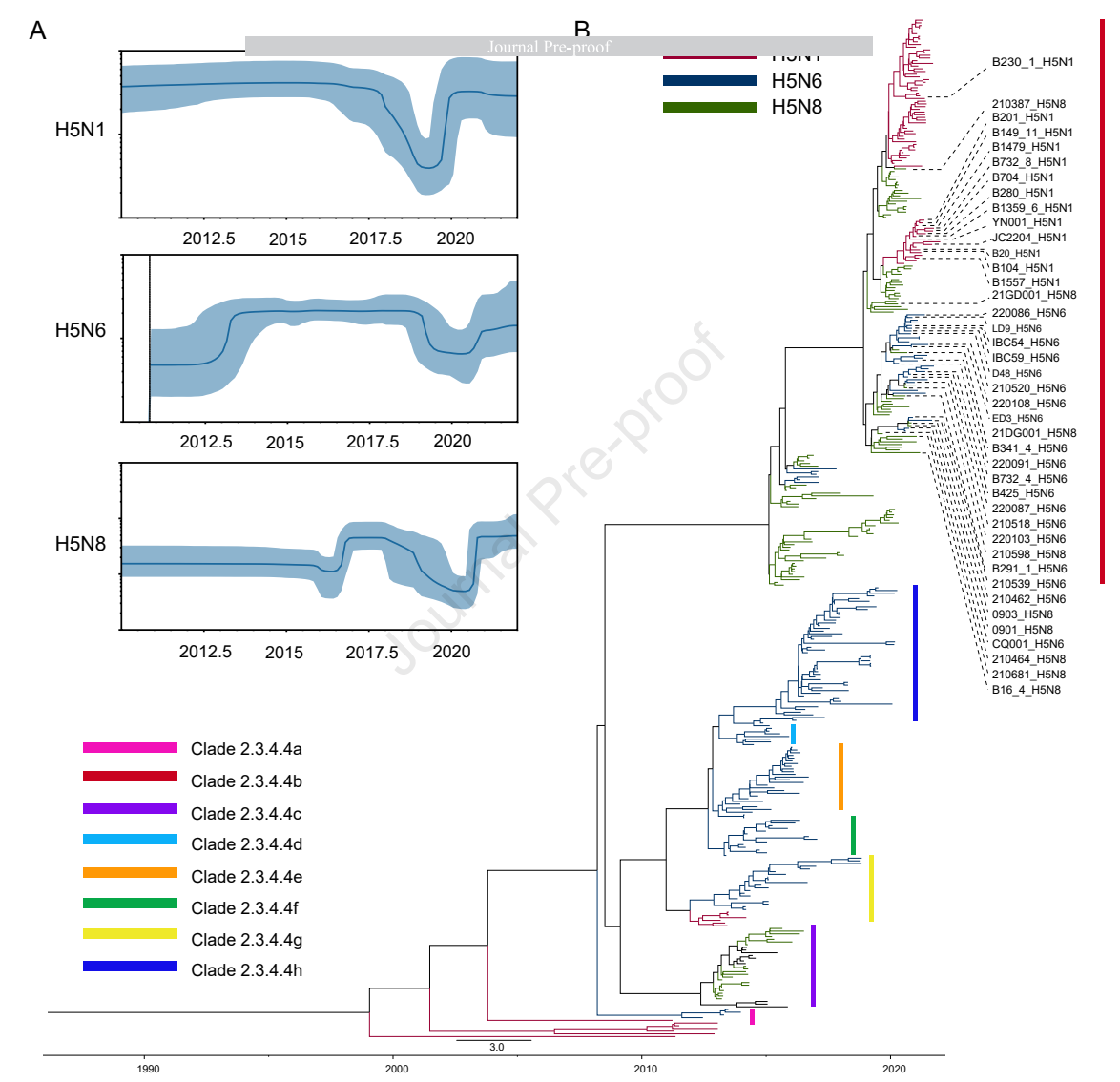

A

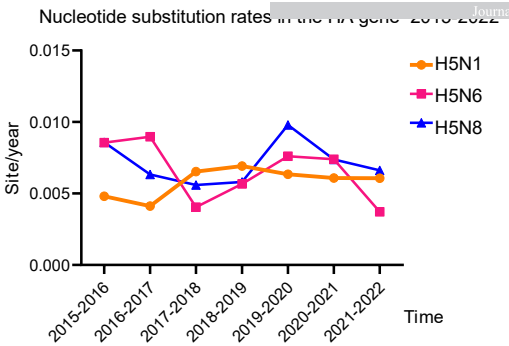

B

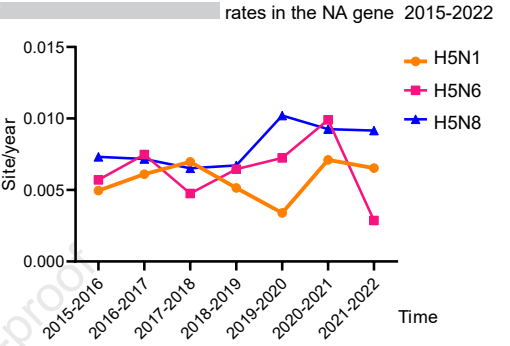

C

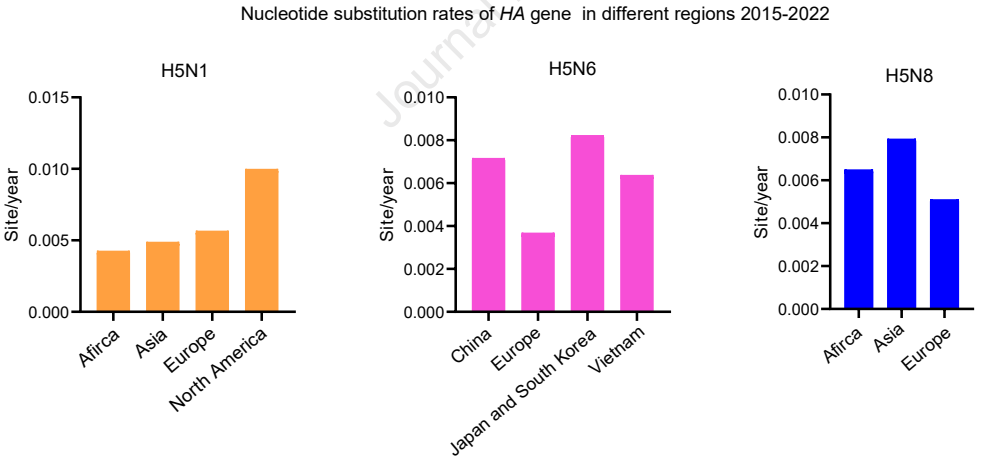

A

B

H5N1

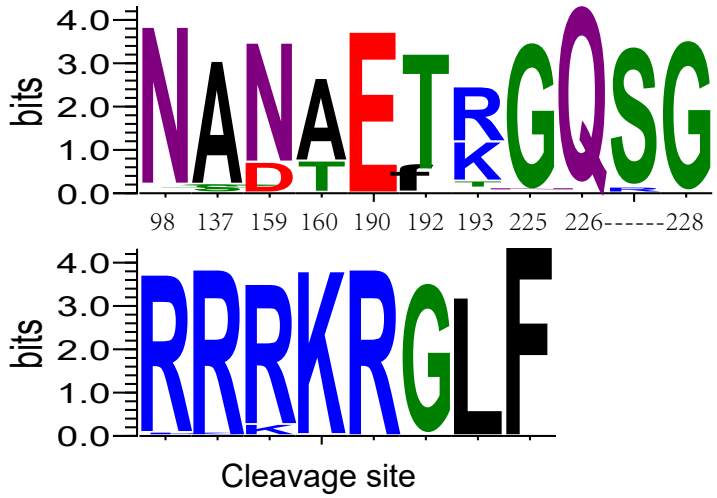

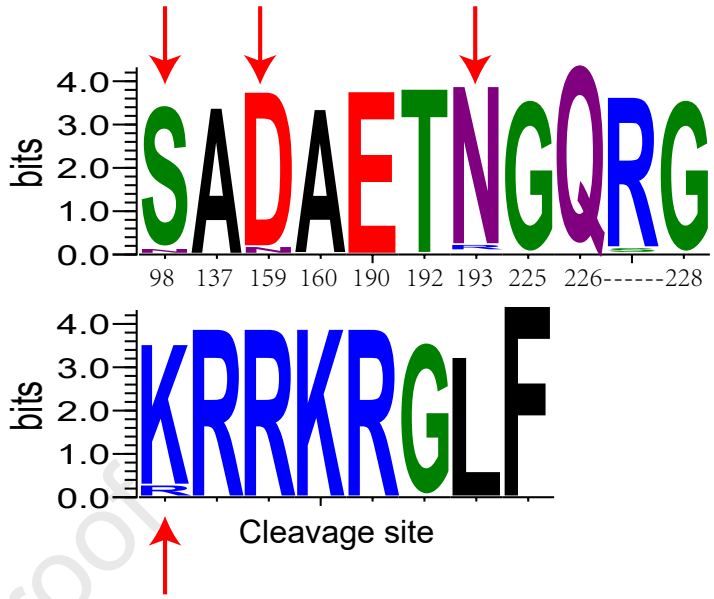

H5N6

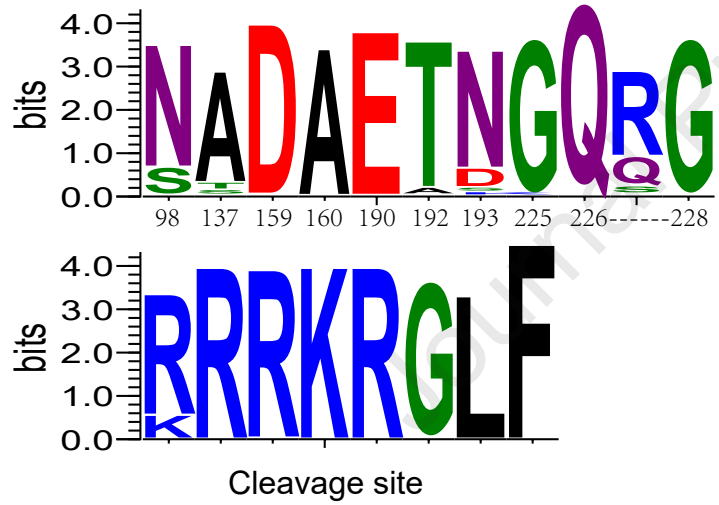

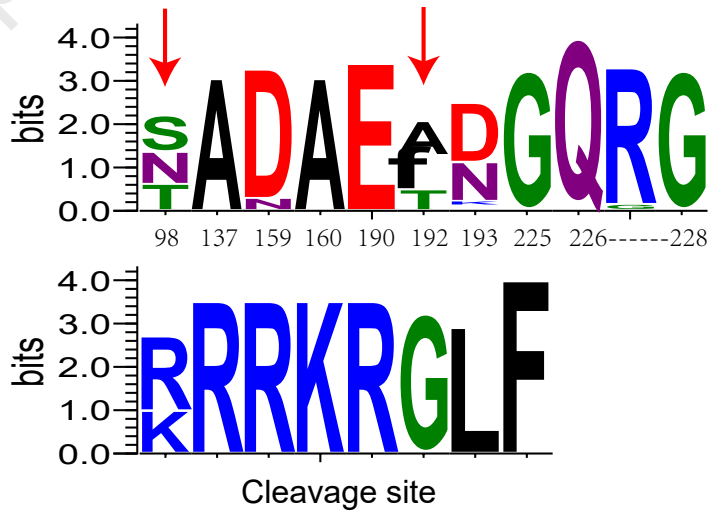

H5N8

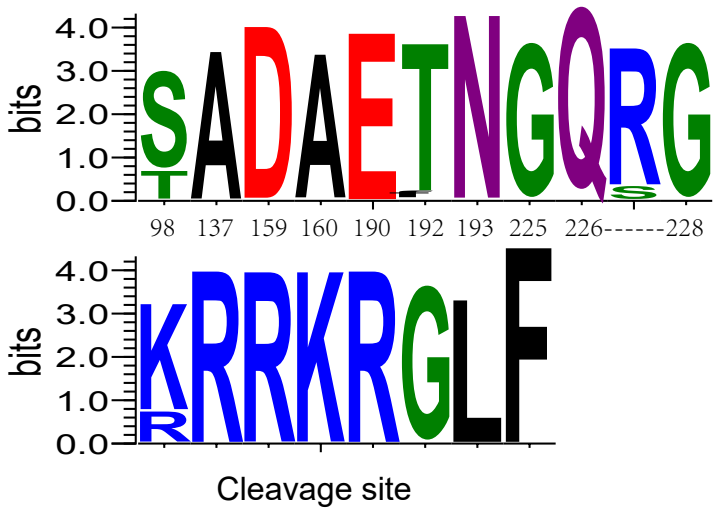

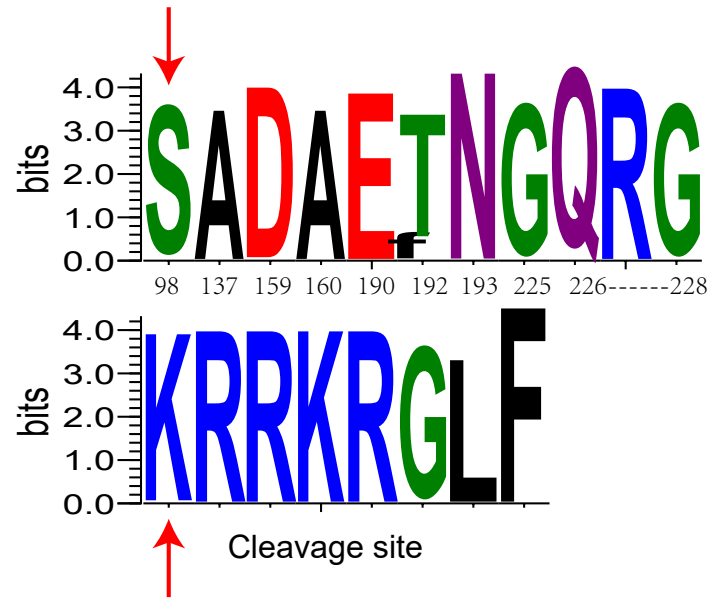

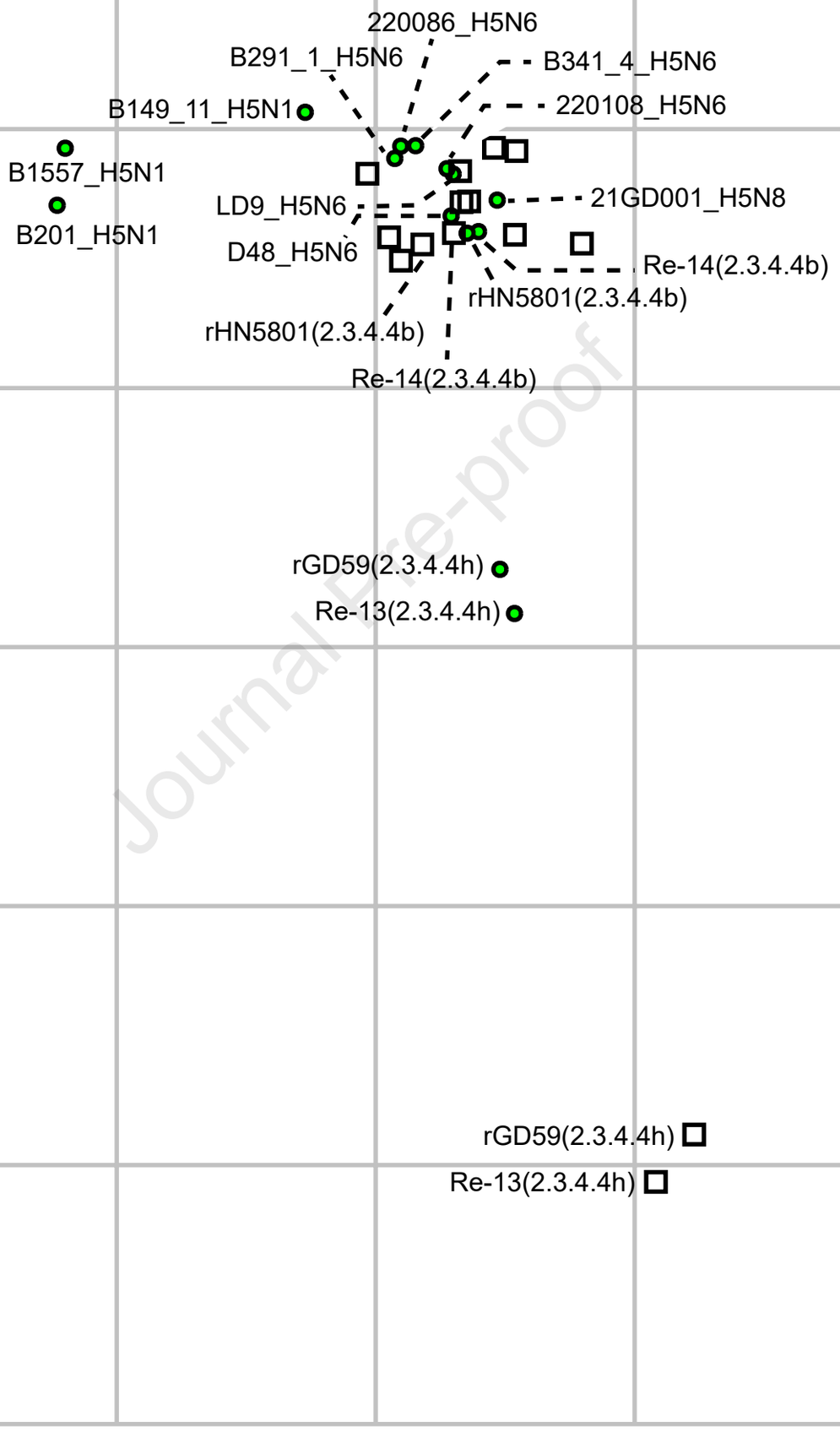

A

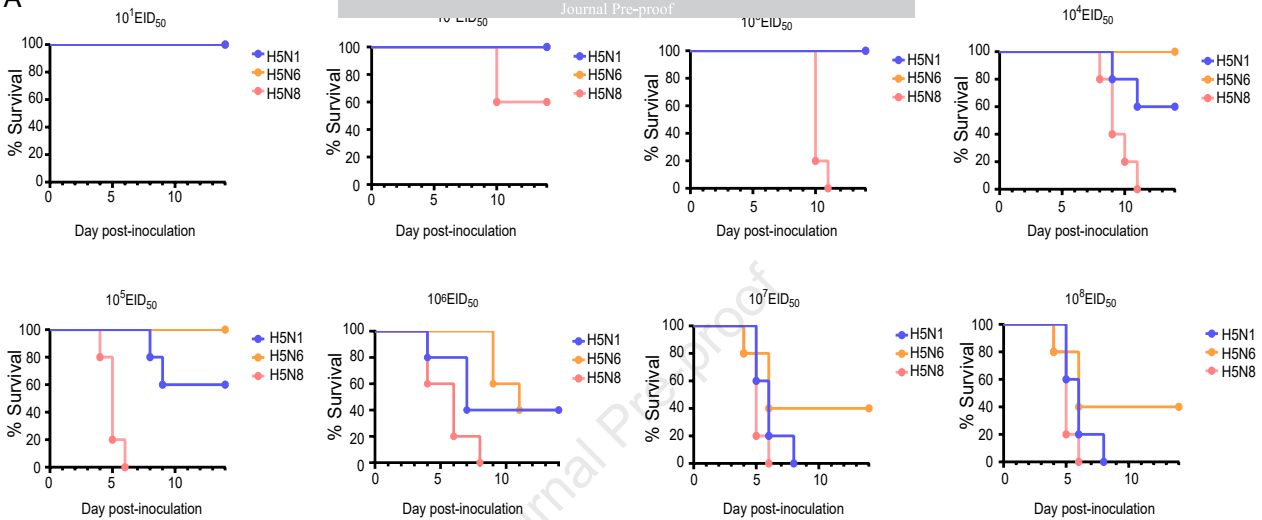

B